Electrocatalysts

DOI: 10.1002/anie.201310597

Electrochemical Synthesis of Tetrahexahedral Rhodium Nanocrystals with Extraordinarily High Surface Energy and High Electrocatalytic Activity**

Neng-Fei Yu, Na Tian, Zhi-You Zhou, Long Huang, Jing Xiao, Yu-Hua Wen, and Shi-Gang Sun**

Abstract: *Noble metal nanocrystals (NCs) enclosed with high-index facets hold a high catalytic activity thanks to the high density of low-coordinated step atoms that they exposed on their surface. Shape-control synthesis of the metal NCs with high-index facets presents a big challenge owing to the high surface energy of the NCs, and the shape control for metal Rh is even more difficult because of its extraordinarily high surface energy in comparison with Pt, Pd, and Au. The successful synthesis is presented of tetrahexahedral Rh NCs (THH Rh NCs) enclosed by {830} high-index facets through the dynamic oxygen adsorption/desorption mediated by square-wave potential. The results demonstrate that the THH Rh NCs exhibit greatly enhanced catalytic activity over commercial Rh black catalyst for the electrooxidation of ethanol and CO.*

Rhodium nanocrystals (Rh NCs) have been widely used as industrial catalysts, typically in applications of fine chemical synthesis, oil refining processes, automobile exhaust purification, and energy conversion technology, owing to their unique properties.[1] Shape manipulation of Rh NCs with high-index facets is an efficient approach for enhancing their catalytic properties,[2] because high-index facets contain a high density of low-coordinated step atoms with high reactivity. However, such shape control is quite challenging owing to the extraordinarily high surface energy of Rh. Convex Rh NCs with high-index facets have not been achieved so far, and there are only a few reports about shape control of Rh NCs enclosed by {111}, {100}, and even {110} facets in the form of tetrahedral, cubes, cuboctahedra, concave cubes, and multipods.[3]

[*] N. F. Yu, Dr. N. Tian, Dr. Z. Y. Zhou, L. Huang, J. Xiao, Prof. S. G. Sun
State Key Laboratory of Physical Chemistry of Solid Surfaces
Department of Chemistry, College of Chemistry and Chemical Engineering, Xiamen University
Xiamen 361005 (China)
E-mail: tnsd@xmu.edu.cn
sgsun@xmu.edu.cn
Y.-H. Wen
Institute of Theoretical Physics and Astrophysics
Department of Physics, Xiamen University (China)

[**] This study was supported by the National Basic Research Program of China (2012CB215500), NSFC (21222310, 21373175, 21361140374, 21321062, and 21229301), Foundation for the Author of National Excellent Doctoral Dissertation of China (201126), and the Ph.D. program of Xiamen University.

Supporting information for this article is available on the WWW under http://dx.doi.org/10.1002/anie.201310597.

It is well-known that the surface energy plays a key role in the shape-controlled synthesis of metal NCs because of the thermodynamic restriction of minimizing total surface energy during the growth of NCs.[4] Figure 1 compares the surface energy of different {hkl} facets and corresponding nanocrystal

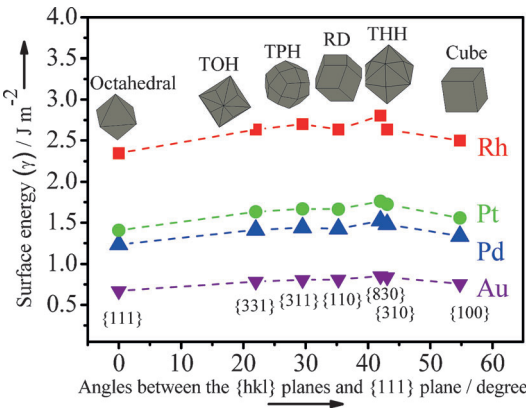

Figure 1. Variation of surface energy of different {hkl} facets and corresponding nanocrystal shapes for noble metal Rh, Pt, Pd, and Au. Shapes: octahedron, trisoctahedron (TOH), trapezohedron (TPH), rhombic dodecahedron (RD), tetrahexahedron (THH), and cube.

shapes for noble metals of Rh, Pt, Pd, and Au. The surface energy data were calculated according to the quantum corrected Sutton–Chen (Q-SC) type many-body potentials, which belong to the embedded-atom method (EAM), and can describe many properties of fcc metals and their alloys as well.[5] According to the value of surface energy, the aforementioned metals can be classified into three grades in the order of $\gamma_{Rh} \gg \gamma_{Pt} \approx \gamma_{Pd} > \gamma_{Au}$. Au has the lowest surface energy, so Au NCs with high-index facets can be readily synthesized by wet-chemical method through preferential adsorption of capping agents to reduce intrinsic surface energy. A wide variety of morphologies of Au NCs with high-index facets have been synthesized, such as trisoctahedron (TOH), tetrahexahedron (THH), truncated-THH, concave hexoctahedron (HOH), rhombic dodecahedron (RD), and truncated ditetragonal prism.[6] For Pt and Pd, they possess moderate surface energy, which is about 2.0 times higher than that of Au. So, it is more difficult to overturn the order of surface energy between low- and high-index facets of Pt and Pd than Au through preferential adsorption of capping agents. As a consequence, it is challenging to use wet chemical methods to synthesize Pt and Pd NCs with high-index facets,

especially convex polyhedral NC. So far, only a few concave shapes of Pt and Pd NC, such as concave cube and concave tetrahedral/trigonal bipyramids, and core–shell structures were achieved by wet chemical methods.[7] In contrast, the electrochemical square-wave-potential (SWP) route has succeeded in a set of morphology of Pt and Pd NCs with high-index faces, including THH, trapezohedron (TPH), and HOH.[8] This indicates clearly that electrochemical route holds a great advantage to synthesize high-energy metal NCs with high-index facets in comparison with wet chemical methods. The merits of the electrochemical route for synthesizing NCs enclosed with high-index facets consist of following aspects: 1) The dynamic oxygen adsorption/desorption mediated by the SWP, which could generate high-index facets on the NCs; 2) the significant inhibition effect in place-exchange between oxygen and metal surface atoms on high-index facets; and 3) the decrease in surface energy of the high-index facets by electrochemical adsorption of hydrogen or oxygen species.[8a,2a] It is worthwhile pointing out that Rh metal possesses the highest surface energy among above-mentioned four noble metals. As illustrated in Figure 1, the surface energy of Rh is more than three times higher over that of Au. Therefore, the electrochemical route could be more efficient to synthesize Rh NCs with high-index facets compared with the wet chemical method.

Herein, we report the successful synthesis of THH Rh NCs enclosed with {830} high-index facets by using electrochemical SWP method. We found that unlike Pt and Pd, the THH Rh NCs can only be obtained in a very narrow potential window (±30 mV) for both upper and lower limits of the SWP through systematical optimization of preparation conditions. We further demonstrated that the high-index facets of THH Rh NCs can promote oxygen adsorption in comparison with commercial Rh black, and then greatly enhance catalytic activity towards electrooxidation of ethanol and carbon monoxide (CO).

The THH Rh NCs were electrodeposited on a glassy carbon (GC, $\phi = 6$ mm) electrode in a solution of 1 mM $Na_3RhCl_6 + 0.1$ M H_2SO_4 (Supporting Information, Figure S1). In brief, crystal nuclei were first generated by the nucleation pulse potential (E_N) at −0.40 V (vs. saturated calomel electrode, SCE) for 40 ms. The growth of crystal nucleus to THH Rh NCs was achieved by SWP ($f = 100$ Hz) with lower potential limit (E_L) at −0.07 V and upper potential limit (E_U) at 0.70 V for a growth time (t_G) of 45 min.

Figure 2a displays a low-magnification SEM image of the as-prepared Rh NCs. It has found that the Rh NCs with THH shape are the dominant products with a typical yield of over 80%. The THH NCs can be considered as a cube with each face capped by a square pyramid. The high-magnification SEM image (Figure 2b) illustrates clearly the perfect THH shape of the Rh NCs, with sharply faceted edges. The particle size distribution was determined by statistics of over 300 Rh THH NCs. As shown in the Supporting Information, Figure S2, the size of the THH Rh NCs varies from 25 to 85 nm with an average of 53.3 nm. We note that Chen et al. reported very recently the synthesis of concave cubes of Rh, and they claimed the formation of {*hk*0} high-index facets.[3e] However, the surface of the concave Rh cubes is rather rough.

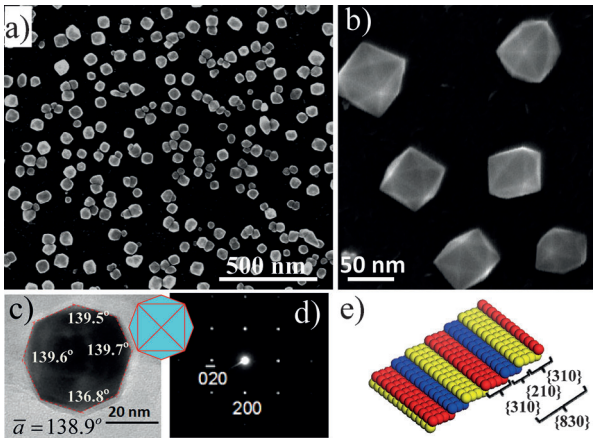

Figure 2. a) Low- and b) high-magnification SEM images of THH Rh NCs obtained at $E_U = 0.70$ V and $E_L = -0.07$ V. c) TEM image and d) SAED pattern of a THH Rh NC along the [001] direction. e) Atomic arranged model of {830} plane.

THH NC is enclosed by 24 {*hk*0} high-index facets. The Miller indices of exposed facets of the THH NCs can be best revealed by imaging the NC along [001] direction, parallel to which 8 of the 24 facets form an octagonal projection (Supporting Information, Figure S3). The Miller indices can be determined by measurement of crystal interfacial angle of α.[8a] Figure 2c displays the typical transmission electron microscopy (TEM) image of a THH Rh NC along the [001] direction, as confirmed by four-fold symmetrical selected-area electron diffraction (SAED) pattern (Figure 2d). The average value of angle α on the projection of the THH Rh NC was measured to be 139.0° (Figure 2c), which are quite close to the theoretical values of $\alpha = 138.9°$ on a THH NC enclosed by {830} facets (Supporting Information, Table S1). The {830} surface is periodically composed of two {310} subfacets followed by a {210} subfacet, as illustrated in Figure 2e. The {830} high-index facets have a large number (4.61×10^{14} cm^{-2}) of step atoms with a low coordination number of six. The reproducibility of the preparation of the THH Rh NCs is fairly good, but the Miller indices of high index facets may vary slightly (α ranging from 137° to 140°).

The formation of THH Rh NCs with high surface energy could be achieved as follows: 1) At E_U, adsorbed oxygen species generated from H_2O dissociation acts as an efficient surface-structure mediator to induce the formation of high-index facets (Supporting Information, Figure S4), as THH Pt NCs we reported previously.[8a] Oxygen adsorbs preferentially on the low-coordinated step atoms and thus decreases the surface energy of high-index facets, because the oxygen binding energy on Rh step atoms is very large (218.1 kJ mol^{-1}),[9] so that high-index facets can be selectively preserved; 2) at E_L, the oxygen species are reductively desorbed and Rh ions are reduced, resulting in the growth of Rh NCs; and 3) the repetitive adsorption and desorption of oxygen at E_U and E_L leads to the formation of the THH Rh NCs.

Although THH Rh NCs can be synthesized by electrochemical SWP method, very precise control of E_L and E_U is required. It was found that even slight change (±0.03 V) of

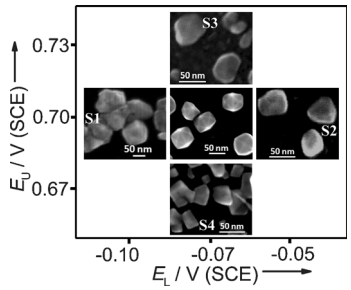

Figure 3. Effect of E_U and E_L on the morphologies of Rh NCs. THH Rh NCs can be obtained at $E_U = 0.70$ V and $E_L = -0.07$ V, and a slight up- or down-shift (ca. 0.03 V) of E_U and E_L results in irregular Rh nanoparticles.

the E_L or E_U potential can result in quite different morphologies, as demonstrated in Figure 3 (for overview SEM images, see the Supporting Information, Figure S5). As shown above in Figure 2, the THH Rh NCs can be obtained at $E_L = -0.07$ V and $E_U = 0.70$ V. The E_L of -0.07 V is near to the onset of Rh electrodeposition on bare GC substrate (Supporting Information, Figure S6). If the E_L was only decreased by 0.03 V from -0.07 to -0.10 V, while keeping the other parameters unchanged, the products (named S1) were mainly irregular nanoparticles and a small amount of aggregates. This may be attributed to that the reduction rate of Rh precursor was too fast at such a negative potential ($E_L = -0.10$ V), resulting in fast growth and then aggregation of Rh NCs. When E_L was increased from -0.07 to -0.05 V, the products (named S2) were also mainly irregular nanoparticles with a few imperfect THH Rh NCs. We further explored the effect of E_U on morphology of Rh NCs. When E_U was increased by only 0.03 V from 0.70 to 0.73 V, the products (named S3) were the mixture of irregular nanoparticles and a small amount of imperfect THH Rh NCs. Even the 0.03 V positive shift of E_U can cause over etching of the Rh surface by adsorbed oxygen, and over dissolution of Rh atoms. When E_U was decreased by 0.03 V from 0.70 to 0.67 V, the products (named S4) were mainly irregular polygon nanoparticles, as the surface reconstruction effects of oxygen adsorption becomes insufficient with such a low E_U value (0.67 V).

The above results suggest that both E_L and E_U can greatly influence the morphology of Rh NCs. The tunable windows of E_U and E_L for the formation of perfect THH Rh NCs are quite narrow (not exceed 30 mV) compared to those of THH Pt NCs and THH Pd NCs (for example, THH Pt NCs can be obtained at tunable SWP windows of 200 mV).[8a,b] That is, an exquisite counterbalance between the etching at E_U and reduction of Rh precursor at E_L is critical to form the perfect THH Rh NCs prepared by the SWP method. The reason may be correlated with the adsorption/desorption characteristic of oxygen species on Rh. As demonstrated in the Supporting Information, Figure S7a, the electrochemical adsorption/desorption of oxygen on Rh is quite irreversible, that is, the potential gap between oxidation and reduction peaks increases greatly with increasing the upper potential limits. In contrast, the reduction of oxygen species on Pt (Supporting Information, Figure S7b) is relatively reversible as compared with Rh. The difference in reversibility for oxygen adsorption/desorption may be correlated to high affinity of Rh to oxygen.[9] As a result, too high value of E_U (> 0.70 V) may result in the insufficient time for oxygen species desorption at the E_L. In our synthetic procedures, the frequency of SWP is 100 Hz, that is, the dwell time at the E_L is 5 ms. As shown in the Supporting Information, Figure S8, the time of 5 ms is not enough to completely reductive desorption of oxygen species on Rh, especially when the adsorption potential of E_U is higher than 0.73 V.

The optimal E_U at 0.70 V may be related to the formation of different oxygen species on Rh. Previously, Jerkiewicz et al. reported that a monolayer OH adsorption on Rh below 0.95 V (*vs* NHE) in 0.5 M H_2SO_4, and multilayer $Rh(OH)_3$ formation after that.[10] The value of 0.95 V (vs. NHE) in 0.5 M H_2SO_4 is equivalent to 0.67 V vs. SCE in 0.1 M H_2SO_4 we used, assuming the formation potential of Rh oxide is independent to reversible hydrogen electrode (RHE) scale. As we proposed previously, site-exchange between noble metal atoms and oxygen atoms (that is, multilayer oxide) that can preferentially occur on low-index facets and disturb them, plays a key role in the formation of high-index facets.[8a,b] Therefore, 0.70 V may be the appropriate potential for the formation of $Rh(OH)_3$ to remove low-index facets, and at the same time to avoid over-etching the surface.

The concentration of Na_3RhCl_6 precursor also plays a key role for the preparation of THH Rh NCs (Supporting Information, Figure S9). Increasing the Na_3RhCl_6 concentration from 1.0 to 2.5 mM will result in a mixture of THH Rh NCs and irregular Rh NCs. Further increasing the Na_3RhCl_6 concentration to 5.0 mM, a large amount of irregular Rh NCs with rough surfaces were produced. When decreasing the concentration of Na_3RhCl_6 from 1.0 to 0.5 mM, THH Rh NCs can still be obtained, but a large number of small Rh NCs with irregular shape were also presented. If the Na_3RhCl_6 concentration was reduced to 0.1 mM, almost no THH Rh NCs were formed.

Electrochemical voltammetry is a powerful method to probe the surface structures of NCs of metals such as Pt, Pd, and Rh. It is known that electric charge of oxygen adsorption is relevant to the quantity of surface step atoms, because the low-coordinated step atoms can promote oxygen adsorption.[11] As a result, a larger current density may correspond to higher step density. Similar to that on Pt, hydrogen and oxygen can also adsorb/desorb on a Rh surface. Figure 4a illustrates typical cyclic voltammograms (CVs) in 0.1 M H_2SO_4 for Rh NCs synthesized by the SWP method, as well as commercial Rh black catalyst. The current was normalized to the electrochemically active surface area (ECSA), which was calculated from the electric charges for electrooxidation of monolayer CO adsorbed on Rh surface.[12a] In Figure 4a, two pairs of characteristic peaks (A1/C1 and A2/C2) correspond to hydrogen desorption/adsorption and oxygen adsorption/desorption, respectively. Clearly, THH Rh NCs can promote the oxygen adsorption in the low potential region. The electric charge density of oxygen adsorption from 0.10 to 0.55 V was measured to be 0.31, 0.20, 0.19, and 0.16 mC cm^{-2} on THH Rh NCs, S2, S1, and commercial Rh black catalyst, respectively, which confirms further that the as-prepared THH Rh NCs have a large number of low-coordinated step atoms. Note that

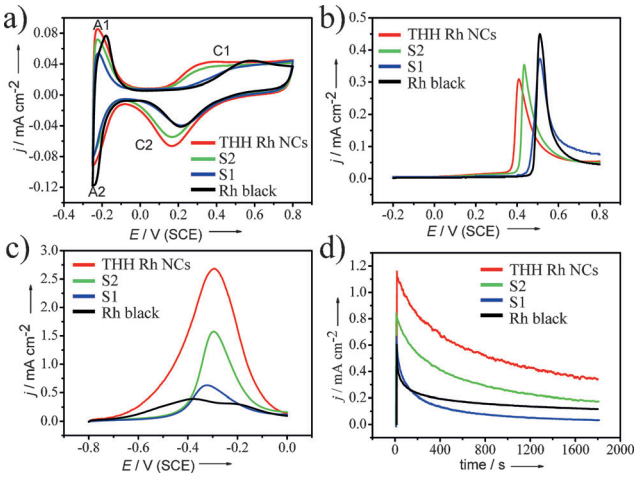

Figure 4. Electrochemical characterization of as-synthesized Rh NCs and commercial Rh black catalyst. a) Cyclic voltammograms (CVs) in 0.1 M H_2SO_4 solution; b) linear sweep voltammograms (LSV) of CO oxidation in 0.1 M H_2SO_4 solution; c) LSVs of ethanol oxidation in 1.0 M ethanol + 1.0 M NaOH solution (scan rate: 50 mV s^{-1}); d) current–time curves for ethanol oxidation at −0.45 V.

although high-index facets have high affinity for oxygen species, they also have high resistance to the formation of multilayer oxide in comparison with {111} facet based on DFT calculations.[13]

Many electrocatalytic reactions, such as electrooxidation of CO and ethanol, are surface-structure sensitive. Herein, the electrooxidation of CO and ethanol was used as test reactions to evaluate the electrochemically catalytic properties of THH Rh NCs. For the CO stripping reaction, linear sweep voltammetry (LSV) was employed to oxidize monolayer CO adsorbed on the Rh surface. Figure 4b shows a characteristic peak of CO oxidation on THH Rh NCs, S2, S1, and commercial Rh black catalyst. It can be clearly seen that both the onset potential and peak potential of CO oxidation increase in the order THH Rh NCs < S2 < S1 < Rh black. The onset potential on THH Rh NCs is 0.36 V, which is about 100 mV negative than that on commercial Rh black (0.46 V), and the peak potential is also about 100 mV more negative on THH Rh NCs (0.40 V) than commercial Rh black (0.51 V). This result demonstrates that the THH Rh NCs with high-index facets are beneficial to CO oxidation, which is in good agreement with previous studies that the Rh surfaces with open surface structure are active for CO stripping.[12]

Ethanol electrooxidation was further investigated on both THH Rh NCs and the other samples. Figure 4c shows the linear sweep voltammograms of ethanol oxidation in 1.0 M NaOH + 1.0 M ethanol solution at room temperature. The peak current density was used to evaluate the catalytic activity. Among all the samples tested, the THH Rh NCs yield the highest electrocatalytic activity of 2.69 mA cm^{-2}, which is 1.7, 4.4, and 6.9 times that of S2, S1, and commercial Rh black catalyst, respectively. Long-term chronoampermetric (CA) measurements were also conducted to fully evaluate the catalytic activity of THH Rh NCs for ethanol oxidation under continuous operating conditions. Figure 4d displays current–time curves recorded at −0.45 V for 1800 s. The THH Rh NCs always displayed a higher catalytic activity than that of commercial Rh black catalyst over the whole time range of CA measurement. At 1800 s, the current density on THH Rh NCs catalyst still maintained a value approximately 1.8 times higher than that of commercial Rh black catalyst. More importantly, the THH Rh NCs are chemically stable, and maintain perfect THH shape after the testing of CO stripping and ethanol electrooxidation (Supporting Information, Figure S10), demonstrating that the THH Rh NCs are stable under catalytic reactions in both acid and alkaline solutions. We further carried out the stability test by 1000 potential cycles between −0.22 and 0.80 V at a scan rate of 100 V s^{-1} in 0.1 M H_2SO_4 (Supporting Information, Figure S11). The CV curves changed little, and the THH shape of Rh NCs was still well preserved, indicating the high electrochemical stability of THH Rh NCs. Considering the very harsh growth conditions (continuous oxidation–reduction induced by the SWP) of THH Rh NCs, it is expected that they have high resistance for electrochemical corrosion.

In summary, the synthesis of THH Rh NCs with extraordinarily high surface energy has been reported by using the electrochemical square-wave potential method without using additional capping agents. The THH Rh NCs are enclosed by {830} high-index facets with high density of low-coordinated step atoms. As a result, electrocatalytic activity for CO and ethanol oxidation, as well as oxygen adsorption at low potential are greatly enhanced on the THH Rh NCs over other Rh nanostructures synthesized in this work. The successful synthesis of THH Rh NCs demonstrates that electrochemical square-wave-potential method is unique for preparing metal NCs with extraordinarily high surface energy. It is worthwhile pointing out that future research will be required to systematically control the shapes (for example, TPH and TOH in Figure 1) of Rh NCs to rationally design and tune their electrocatalytic performance.

Experimental Section

$Na_3RhCl_6 \cdot 12H_2O$ (99.99%) and commercial Rh black catalyst (Johnson Matthey) were purchased from Alfa Aesar. Sulfuric acid (H_2SO_4, GR reagent), sodium hydroxide (NaOH, GR reagent), and ethanol (CH_3CH_2OH, GR reagent) were purchased from China Medicine Shanghai Chemical Reagent Corp. All solutions were prepared with Millipore water (18.2 MΩ cm) provided by a Milli-Q Lab apparatus (Nihon Millipore Ltd.). Glassy carbon rod (GC, ϕ = 6 mm) was purchased from Takai Carbon Co., Ltd., Tokyo, Japan.

The electrodeposition bath for synthesis of THH Rh NCs was prepared by adding 150 mg $Na_3RhCl_6 \cdot 12H_2O$ to 250 mL 0.1 M H_2SO_4 solution with stirring to dissolve $Na_3RhCl_6 \cdot 12H_2O$. The fresh solution presented purple, and then it was aged at 30 °C until it become yellow. The aging is very important for the synthesis of THH Rh NCs. Prior to the electrodeposition, the GC electrode was mechanically polished using successively alumina powder of size 5, 1, and 0.3 μm. It was then cleaned in an ultrasonic bath. Electrochemical preparation and characterizations were carried out in a standard three-electrode cell working with a 263A potentiostat/galvanostat (EG&G). A saturated calomel electrode (SCE) was used as reference electrode, and all potentials are quoted versus the SCE scale. The THH Rh NCs were electrodeposited on the GC electrode by using the programmed electrochemical square wave potential method at room temperature (about 25 °C) in above aged Na_3RhCl_6 solution. The morphology and structure of Rh NCs were characterized by scanning electron

microscopy (SEM, Hitachi S-4800) and transmission electron microscopy (TEM, JEM-2100).

Received: December 6, 2013
Revised: February 21, 2014
Published online: April 1, 2014

Keywords: electrocatalysis · ethanol electrooxidation · high-index facets · nanocrystals · rhodium

[1] a) H. S. Gandhi, G. W. Graham, B. W. McCabe, *J. Catal.* **2003**, *216*, 433; b) Y. Zhang, M. E. Grass, W. Huang, G. A. Somorjai, *Langmuir* **2010**, *26*, 16463; c) Y. Zhang, M. Janyasupab, C. W. Liu, J. Xu, C. C. Liu, *Adv. Funct. Mater.* **2012**, *22*, 145; d) J. L. Pellegatta, C. Blandy, V. Colliere, R. Choulkroun, B. Choudret, P. Cheng, K. Philppot, *J. Mol. Catal. A* **2002**, *177-190*, 433; e) T. J. Yoon, J. I. Kim, J. K. Lee, *Inorg. Chim. Acta* **2003**, *345*, 228.

[2] a) N. Tian, Z. Y. Zhou, S. G. Sun, *J. Phys. Chem. C* **2008**, *112*, 19801; b) Z. Y. Zhou, N. Tian, I. Broadwell, S. G. Sun, *Chem. Soc. Rev.* **2011**, *40*, 4167; c) C. Burda, X. B. Chem, R. Narayanan, M. A. El-Sayed, *Chem. Rev.* **2005**, *105*, 1025; d) R. Narayanan, M. A. El-Sayed, *Nano Lett.* **2004**, *4*, 1343; e) K. M. Bratlie, H. Lee, K. Komvopoulos, P. D. Yang, G. A. Somorjai, *Nano Lett.* **2007**, *7*, 3097.

[3] a) J. D. Hoefelmeyer, K. Niesz, G. A. Somorjai, T. D. Tilley, *Nano Lett.* **2005**, *5*, 435; b) S. M. Humphrey, M. E. Grass, S. E. Habas, K. Niesz, G. A. Somorjai, T. D. Tilley, *Nano Lett.* **2007**, *7*, 785; c) H. Zhang, W. Y. Li, M. S. Jin, J. Zeng, T. Yu, D. Yang, Y. N. Xia, *Nano Lett.* **2011**, *11*, 898; d) K. H. Park, K. Jang, H. J. Kim, S. U. Son, *Angew. Chem.* **2007**, *119*, 1170; *Angew. Chem. Int. Ed.* **2007**, *46*, 1152; e) Y. Chen, Q.-S. Chen, S.-Y. Peng, Z. Wang, *Chem. Commun.* **2014**, *50*, 1662.

[4] Y. D. Yin, A. P. Alivisatos, *Nature* **2005**, *437*, 664.

[5] a) T. Cagin, Y. Kimura, Y. Qi, H. Li, H. Ikeda, W. L. Johnson, W. A. Goddard, *Mater. Res. Soc. Symp. Proc.* **1999**, *554*, 43; b) Y. N. Wen, J. M. Zhang, *Solid State Commun.* **2007**, *144*, 163.

[6] a) D. Wang, Y. Liu, T. You, *CrystEngComm* **2012**, *12*, 4028; b) D. Y. Kim, S. H. Im, O. O. Park, *Cryst. Growth Des.* **2010**, *10*, 3321; c) T. T. Tran, X. Lu, *J. Phys. Chem. C* **2011**, *115*, 3638; d) Y. Y. Ma, Q. Kuang, Z. Y. Jiang, Z. X. Xie, R. B. Huang, L. S. Zheng, *Angew. Chem.* **2008**, *120*, 9033; *Angew. Chem. Int. Ed.* **2008**, *47*, 8901; e) G. H. Jeong, M. Kim, Y. W. Lee, W. Choi, W. T. Oh, Q. H. Park, S. W. Han, *J. Am. Chem. Soc.* **2009**, *131*, 1672; f) T. Ming, W. Feng, Q. Tang, F. Wang, L. Sun, J. Wang, C. Yan, *J. Am. Chem. Soc.* **2009**, *131*, 16350; g) J. Zhang, M. R. Langille, M. L. Personick, K. Zhang, S. Y. Li, C. A. Mirkin, *J. Am. Chem. Soc.* **2010**, *132*, 14012.

[7] a) X. Q. Huang, Z. P. Zhao, J. M. Fan, N. F. Zheng, *J. Am. Chem. Soc.* **2011**, *133*, 4718; b) M. S. Jin, H. Zhang, Z. X. Xie, Y. N. Xia, *Angew. Chem.* **2011**, *123*, 7996; *Angew. Chem. Int. Ed.* **2011**, *50*, 7850; c) T. Yu, D. Y. Kim, H. Zhang, Y. N. Xia, *Angew. Chem.* **2011**, *123*, 2825; *Angew. Chem. Int. Ed.* **2011**, *50*, 2773; d) Y. Yu, Q. B. Zhang, B. Liu, J. Y. Lee, *J. Am. Chem. Soc.* **2010**, *132*, 18258; e) H. Lin, Z. Lei, Z. Jiang, C. Hou, D. Y. Liu, M. Xu, Z. Tian, Z. Xie, *J. Am. Chem. Soc.* **2013**, *135*, 9311.

[8] a) N. Tian, Z. Y. Zhou, S. G. Sun, Y. Ding, Z. L. Wang, *Science* **2007**, *316*, 732; b) N. Tian, Z. Y. Zhou, N. F. Yu, L. Y. Wang, S. G. Sun, *J. Am. Chem. Soc.* **2010**, *132*, 7580; c) Y. Li, Y. X. Jiang, M. H. Chen, H. G. Liao, R. Huang, Z. Y. Zhou, N. Tian, S. P. Chen, S. G. Sun, *Chem. Commun.* **2012**, *48*, 9531; d) J. Xiao, S. Liu, N. Tian, Z. Y. Zhou, H. X. Liu, B. B. Xu, S. G. Sun, *J. Am. Chem. Soc.* **2013**, *135*, 18754.

[9] N. Seriani, F. Mittlendorfer, *Condens. Matter* **2008**, *20*, 184023.

[10] G. Jerkiewicz, J. J. Borodzinski, *Langmuir* **1993**, *9*, 2202.

[11] N. Furuya, S. Koide, *Surf. Sci.* **1989**, *220*, 18.

[12] a) T. H. M. Housmans, J. M. Feliu, M. T. M. Koper, *J. Electroanal. Chem.* **2004**, *572*, 79; b) F. J. Vidal-Iglesias, J. Solla-Gullón, J. M. Campińa, E. Herrero, A. Aldaz, J. M. Feliu, *Electrochim. Acta* **2009**, *54*, 4459; c) T. H. M. Housmans, C. G. M. Hermse, M. T. M. Koper, *J. Electroanal. Chem.* **2007**, *607*, 69.

[13] Y. H. Fang, Z. P. Liu, *J. Phys. Chem. C* **2010**, *114*, 4057.

